Clinical and Experimental Medicine (2026) 26:188
https://doi.org/10.1007/s10238-026-02113-7

RESEARCH

Single-cell profiling reveals MIF-mediated immune evasion and CD8 + T cell exhaustion in relapsed multiple myeloma

Jing Ma[1,2] · Shuang Gao[1] · Su Liu[1] · Lin Chen[1] · Li Lin[1] · Zhiying Zhang[1] · Zhigang Zhao[3] · Qian Li[2]

Received: 12 November 2025 / Accepted: 17 February 2026

Abstract

Multiple myeloma (MM) is a heterogeneous hematologic cancer marked by clonal plasma cell expansion in the bone marrow. Although treatments have improved, relapse remains common due to clonal evolution, tumor microenvironment changes, ultimately leading to drug resistance. This study utilized single-cell RNA sequencing data analysis to explore immune microenvironment dynamics during MM progression and relapse, aiming to uncover key pathways and cellular interactions correlated with disease relapse. ScRNA-seq data from 20 MM patients (10 primary, 2 remission, 8 relapsed) from the GEO dataset GSE223060 were analyzed. After quality control and batch correction, cells were clustered and annotated. Differential gene expression and functional enrichment analyses were conducted to explore cellular functions. Pseudotime analysis was used to trace plasma cell differentiation, and cell–cell communication was analyzed. Immunohistochemistry and flow cytometry were used for validation.60,234 high-quality single cells were classified into 12 distinct populations. Relapsed MM showed increased T cell infiltration and decreased plasma cells. Relapsed samples had more regulatory T cells (Tregs) and impaired CD8 + T cells. MIF was identified as a key regulator in plasma cell evolution, linked to B cell receptor and interferon-alpha signaling. Enhanced MIF pathway activity was noted between plasma cells and CD8 + T cells in relapsed MM. Increased MIF expression was confirmed in relapsed tissues. Our findings reveal profound immune microenvironment remodeling in relapsed MM, characterized by MIF-mediated signaling, NF-κB suppression, and $CD8^+$ T cell dysfunction. These results provide new insights into the mechanisms of MM relapse and highlight potential therapeutic targets for preventing disease relapse.

Keywords Multiple myeloma · Relapse · Single-cell RNA sequencing · Immune microenvironment · MIF · NF-κB

Introduction

Multiple myeloma (MM) is a genetically heterogeneous hematologic malignancy characterized by the proliferation of clonal plasma cells in the bone marrow [1, 2]. According to the Cancer Statistics 2024 report, an estimated 35,780 new cases of MM are projected to occur in the United States, with an associated mortality of approximately 12,540 deaths [3]. Despite advances in therapeutic strategies, including proteasome inhibitors and immunomodulatory drugs [4], relapse remains a major clinical challenge [5]. The high recurrence rate in MM patients is attributed to clonal evolution, tumor microenvironment (TME) remodeling, and the emergence of drug-resistant subclones [1, 6, 7]. Thus, understanding the molecular mechanisms driving relapse is critical for developing targeted therapies and improving patient outcomes.

✉ Zhigang Zhao
goodluckzho001@163.com

✉ Qian Li
liqtj@163.com

[1] Department of Hematology and Blood and Marrow Transplantation, Tianjin Cancer Hospital Airport Hospital, National Clinical Research Center for Cancer, No. 99, Dongwu Road, Tianjin Airport Economic Zone, Tianjin 300300, China

[2] Department of Hematology , Tianjin Medical University Cancer Institute & Hospital, National Clinical Research Center for Cancer, Tianjin's Clinical Research Center for Cancer, Tianjin 300060, China

[3] Department of Medical Oncology, Tianjin First Central Hospital, School of Medicine Nankai University, No. 24, Fukang Road, Nankai District, Tianjin 300192, China

Published online: 08 March 2026

Single-cell RNA sequencing (scRNA-seq) has emerged as a highly effective tool for examining cellular diversity and intercellular interactions within the TME [8, 9]. Its application in MM research has revealed remarkable complexity within the TME, identifying distinct cellular subpopulations that critically influence tumor progression, immune evasion, and resistance to therapy [10, 11]. ScRNA-seq indicates that the most significant differences between MM patients and healthy donors (HD) are localized to malignant plasma cell clusters, which exhibit mitochondrial dysfunction, enhanced proliferative capacity, and marked genomic instability, characterized by elevated copy number variation (CNV) scores and mutated gene expression profiles [11]. The MM TME is further characterized by an expanded population of $CD8^+$ terminally differentiated effector memory T cells (Temra), which exhibit features of cellular senescence and partial exhaustion [12].

Striking molecular distinctions emerge when comparing patients with newly diagnosed multiple myeloma (NDMM) and those with relapsed/refractory MM (RRMM) through scRNA-seq. PRMM specimens demonstrate unique transcriptional signatures associated with mitochondrial stress response, endoplasmic reticulum stress pathways, and proteasomal activity [13]. The relapsed/refractory MM microenvironment exhibits even greater complexity, with S100A9 + plasma cell subsets showing a strong association with 1q21 amplification and distinct patterns of immune checkpoint expression and drug sensitivity [14]. These aggressive clones remodel the bone marrow niche through cytokine overproduction and cellular crosstalk, creating an immunosuppressive milieu enriched with PD1 + γδ T cells, tumor-associated macrophages, and depleted hematopoietic progenitors [15]. While these studies have significantly advanced our understanding of MM biology, a critical knowledge gap remains regarding the comprehensive characterization of intratumoral and intertumoral heterogeneity between primary and relapsed disease sites. Therefore, understanding the cellular and molecular heterogeneity within and between primary and relapsed MM tumors is essential for advancing our knowledge of disease progression.

In this study, we analyzed data derived from scRNA-seq analysis of bone marrow samples from MM patients, comparing primary, remission, and relapsed cases. We employed scRNA-seq to characterize the dynamic changes in cellular composition, transcriptional profiles, and intercellular communication networks during disease progression. Our research revealed key molecular and cellular alterations associated with myeloma relapse, highlighting a profound rewiring of the TME.

Materials and methods

Data collection and processing

The scRNA-seq data (GSE223060) used in this study were obtained from the Gene Expression Omnibus (GEO) database (https://www.ncbi.nlm.nih.gov/geo/), comprising bone marrow samples from 20 patients with MM, including 10 primary, 2 remission, and 8 relapse cases. The clinical characteristics of the patients in each group are summarized in Table 1.

The scRNA-seq data were processed using Seurat (v4.1.1). Cells with mitochondrial content exceeding 10%, hemoglobin content exceeding 5%, or expressing fewer than 200 or more than 5,000 genes were filtered out. Potential doublets were identified and removed using the DoubletFinder in the R package. Batch effects were corrected via Harmony [16] using the RunHarmony function. Data normalization, cell clustering, and dimensional reduction were performed with the Seurat package. The "FindVariableFeatures" function was employed to select 2,000 highly variable genes from the corrected expression matrix. Subsequently, principal component analysis (PCA) was performed using the "RunPCA" function, with the top 20 principal components retained for further analysis. Cell clusters were generated using the "FindClusters" function (resolution = 0.6) and visualized via UMAP (RunUMAP). Cell populations were annotated based on canonical marker genes and reference datasets from CellMarker 2.0.

Differential gene expression and functional enrichment analyses

Differentially expressed genes (DEGs) were identified for each cluster using the "FindMarkers" function in Seurat. Functional enrichment analysis of these DEGs was performed using the R package "clusterProfiler" (v4.8.2), which included both Gene Ontology (GO) and Kyoto Encyclopedia of Genes and Genomes (KEGG) analyses [17]. Significantly enriched GO terms and KEGG pathways were screened using $p < 0.05$.

Pseudotime trajectory analysis

Monocle (v2.28.0) [18] was employed to construct pseudotime trajectories based on the gene expression profiles of plasma cells. After dimensionality reduction and cell ordering, all plasma cells were projected and ordered into trajectories with distinct branches, with cells within the same branch considered to be in the same cellular state. Subsequently, Branched Expression Analysis Modeling (BEAM) was conducted to identify genes with branch-dependent

Table 1 Clinical data of each group of patients

		Patient id	Age	Gender	Race	ISS stage	Treatment	TTPD in months
27522_1	Primary	27522	69	Male	White	2	KRD x 4; ASCT; IRD consolidation x 4 ; Ixa/Len maintenance	32.73
27522_2	Remission-1							
27522_3	Relapse-1							
27522_4	Relapse-2							
27522_5	Remission-2							
27522_6	Relapse-3							
37692_2	Primary	37692	68	Male	White	1	Unknown	NA
47491_2	Primary	47491	68	Male	White	UNK	Unknown	NA
56203_1	Primary	56203	63	Female	White	3	VRD x 3; ASCT; Len maintenance	16.48
56203_2	Relapse-1							
57075_3	Relapse-1	57075	62	Female	White	2	VCD+Rituximab x 5; ASCT; VCD x 2	42.34
58408_2	Primary	58408	53	Male	White	UNK	RVD+Daratumamab x 4; ASCT	7.73
59114_1	Primary	59114	49	Male	White	2	KRD x 4; ASCT; KRD maintenance	44.57
59114_4	Relapse-1							
60359_1	Primary	60359	57	Male	White	1	VD x 3; ASCT; Len maintenance	33.85
60359_2	Relapse-1							
77570	Primary	77570	66	Female	White	1	VRD-Daratumamab x 4; ASCT; VRD-Daratumamab x2; Dara/Len Maintenance	34.34
81012_1	Primary	81012	59	Female	White	1	VRD x 4; ASCT; Len maintenance	26.45
81012_2	Relapse-1							
83942	Primary	83942	63	Male	White	3	Unknown	NA

expression patterns. These branch-dependent genes facilitate the exploration of mechanisms underlying cell fate determination.

Cell–cell interaction analysis

The CellChat algorithm (v2.28.0) was utilized to investigate potential interactions among different cell types. A merged Seurat object, encompassing plasma cells and other cell types within the TME, served as the input for the algorithm. Following the creation of the CellChat object, a reference database was established based on secreted signaling pathways. The functions computeCommunProb and computeCommunProbPathway were employed to infer specific receptor-ligand interactions and communication probabilities among distinct cell types, respectively.

Immunohistochemical analysis

Human tumor and adjacent normal tissue specimens were fixed in 4% formaldehyde, paraffin-embedded, and sectioned into 5 μm thick slices using a microtome. Following deparaffinization with xylene, tissue sections were rehydrated through a graded ethanol series. Antigen retrieval was performed using a citric acid-based buffer (Fuzhou Maixin Biotechnology Development Co., Ltd., China). To quench endogenous peroxidase activity, sections were treated with a peroxidase blocking reagent (Beijing Zhongshan Jinqiao Biotechnology Co., Ltd., China) for 10 min at room temperature. After three 3 min washes with PBS, nonspecific binding was blocked with 10% goat serum. Sections were then incubated overnight at 4 °C with a primary antibody against MIF (1:200 dilution; PA5-60,942, Thermo Fisher Scientific, USA). Following PBS washes, sections were incubated with horseradish peroxidase (HRP)-conjugated secondary antibody for 30 min at 25 °C. Immunoreactivity was visualized using 3,3′-diaminobenzidine (DAB) substrate (10 min), and nuclei were counterstained with hematoxylin for 2 min. Stained sections were imaged under a light microscope (Zeiss, Germany). This study has garnered approval from the Medical Ethics Committee of Tianjin Cancer Hospital Airport Hospital (IREC number: LWK-2025–0012).

Flow cytometry detection

Peripheral blood samples were obtained from patients with primary and relapsed MM. Mononuclear cells were isolated and washed once with PBS. For surface staining, cells were incubated with antibody cocktails from the Flow Cytometry CD45/CD4/CD8/CD3 Detection Kit (6,607,013, Beckman, USA) according to the manufacturer's instructions. All staining procedures were performed in FACS buffer (PBS supplemented with 1% FBS and 5 mM EDTA) for 30 min on ice. After staining, cells were washed and resuspended in FACS buffer. Flow cytometric data were acquired using a Flow Cytometer (BD FACSCanto II, USA) and analyzed with FlowJo software (Treestar).

Cytokine analysis

Peripheral blood samples were obtained from patients with primary and relapsed MM. Plasma was separated within 4 h of collection using Ficoll-Hypaque density gradient centrifugation (Sigma, USA). Selected cytokines (IL-2, IL-4, IL-6, IL-10, TNF-α, and IFN-γ) were quantified using a Human Six-Cytokine Detection Kit (JOINSTAR, China) according to the manufacturer's instructions, and analyzed on the iMatrix 100 flow-through chemiluminescence analyzer. Flow cytometry data were analyzed using FlowJo software (Treestar).

Statistical analysis

Continuous variables were analyzed using the independent Mann–Whitney U test (two-group) or the Kruskal–Wallis test (three groups), as appropriate. Categorical variables were compared using the chi-square test. All statistical analyses were performed using R software (version 4.0.5). A two-tailed P-value <0.05 was considered statistically significant.

Results

Single-cell profiling uncovers immune microenvironment remodeling in MM relapse

To delineate the dynamic molecular and cellular landscape governing MM initiation and progression, we initially acquired scRNA-seq data from 20 MM specimens in the GSE223060 dataset, including 10 primary, 2 remission, and 8 relapsed cases (Fig. 1A, B). Following quality control, a total of 60,234 high-quality single cells were retained for subsequent analysis. These cells were processed through dimensionality reduction and clustering algorithms, which identified 19 discrete cell clusters (Fig. 1C). Based on canonical marker gene expression patterns, the 19 initial clusters were biologically annotated into 12 distinct cell populations: T cells, CD14+monocytes, plasma cells, NK cells, CD16+monocytes, B cells, megakaryocytes, proliferating cells, neutrophils, myeloid dendritic cells (mDCs), macrophages, and plasmacytoid dendritic cells (pDCs) (Fig. 1D, E). Comparative analysis between primary and relapsed groups revealed T cells, CD14+monocytes, and plasma cells as the three most abundant populations (Fig. 1F). Next, we analyzed the cell counts across the primary, remission, and relapsed groups, showing that the primary group contained the highest number of cells, while the remission group had the lowest (Fig. 1G). The proportional distribution of each cell type across individual samples was further quantified (Fig. 1H), with detailed sample-specific proportions provided in Table S1. Notably, we observed a significant increase in the proportion of T cells and a significant decrease in the proportion of plasma cells in relapsed samples compared to primary samples (Fig. 1I, J).

Single cell transcriptional analysis of T cells during MM relapse

To further elucidate the role of T cell heterogeneity in MM progression, we performed a sub-clustering analysis on T cells. After dimensionality reduction and clustering, we identified 8 distinct T cell clusters (Fig. 2A, B), which were further annotated into 4 major subsets based on canonical marker gene expression: CD4+T cells, CD8+T cells, CD4+regulatory T cells (Tregs), and naïve T cells (Fig. 2C, D). All T cell subsets were shared across primary, remission, and relapsed MM samples, but exhibited heterogeneous proportions (Fig. 2A). Moreover, we found that the abundance of CD8+T cells was elevated in remission samples, while the abundance of Treg cells was increased in relapsed samples (Fig. 2E, F). This phenotypic shift likely reflects enhanced tumoricidal capacity of the immune system in phased patients, mediated by CD8+T cell expansion. Conversely, the pronounced accumulation of immunosuppressive Tregs in relapsed samples suggests a tumor-permissive microenvironment characterized by impaired immune surveillance. Such Treg-dominated immunosuppression may facilitate immune escape, ultimately promoting tumor cell survival and dissemination.

To further investigate the functional heterogeneity of T cell subsets, we analyzed the expression profiles of key effector molecules across primary, remission, and relapsed samples. Notably, CD8+T cells from primary samples exhibited significantly higher expression of IFNγ—a pivotal immunomodulatory cytokine that enhances immune cell activation, promotes tumor cell apoptosis, and shapes the TME—compared to relapsed samples (Fig. 2G). This finding suggests that CD8+T cells in primary MM maintain robust cytotoxic functionality, capable of mounting effective anti-tumor responses through IFNγ production. In contrast, the attenuated IFNγ expression in relapsed CD8+T cells implies a progressive loss of cytotoxic potential, likely driven by immunosuppressive mechanisms within the TME (e.g., Treg-mediated suppression). We further scored T cell exhaustion across different T cell subtypes for each group and found that the exhaustion score was significantly higher in the relapsed group than in the primary group (Fig. 2H). Such functional impairment may compromise tumor cell clearance, ultimately fostering immune evasion and disease recurrence.

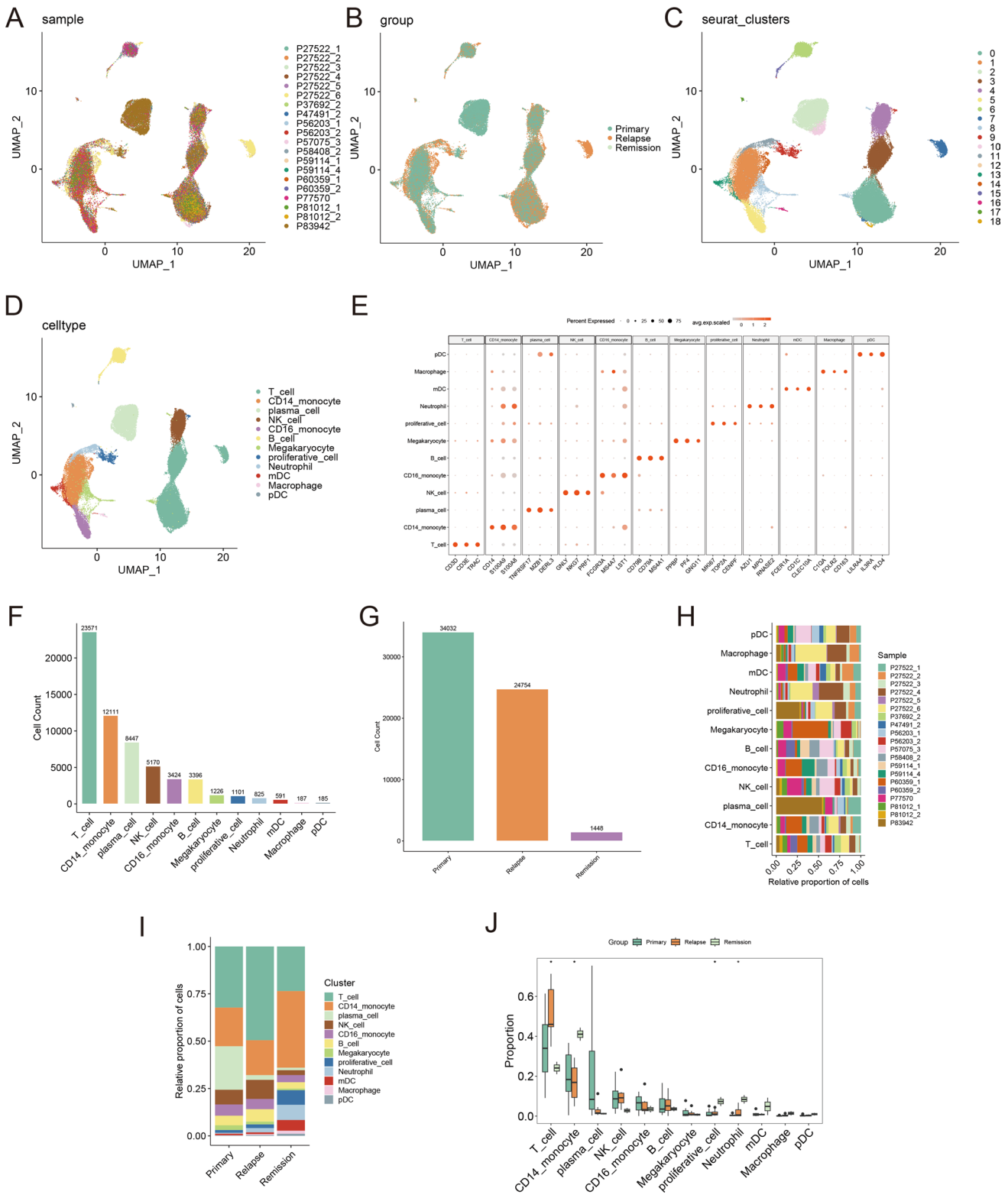

Fig. 1 Single-cell transcriptomics revealed distinct cellular compositions in multiple myeloma (MM) samples. **A** UMAP dimensionality reduction analysis showing the distribution of cells in each sample. **B** Results of cell grouping. **C** Results of cell clusters. **D** The results of cell annotation. **E** The expression of the marker gene in different cell types. **F** The number of different cell types in MM samples. **G** The cell counts across the primary, relapsed, and remission groups. **H** Cell type composition across individual samples. **I** The proportion of different cell types in primary and relapsed MM samples. **J** The proportion differences of various cells in primary and relapsed MM. * $p<0.05$

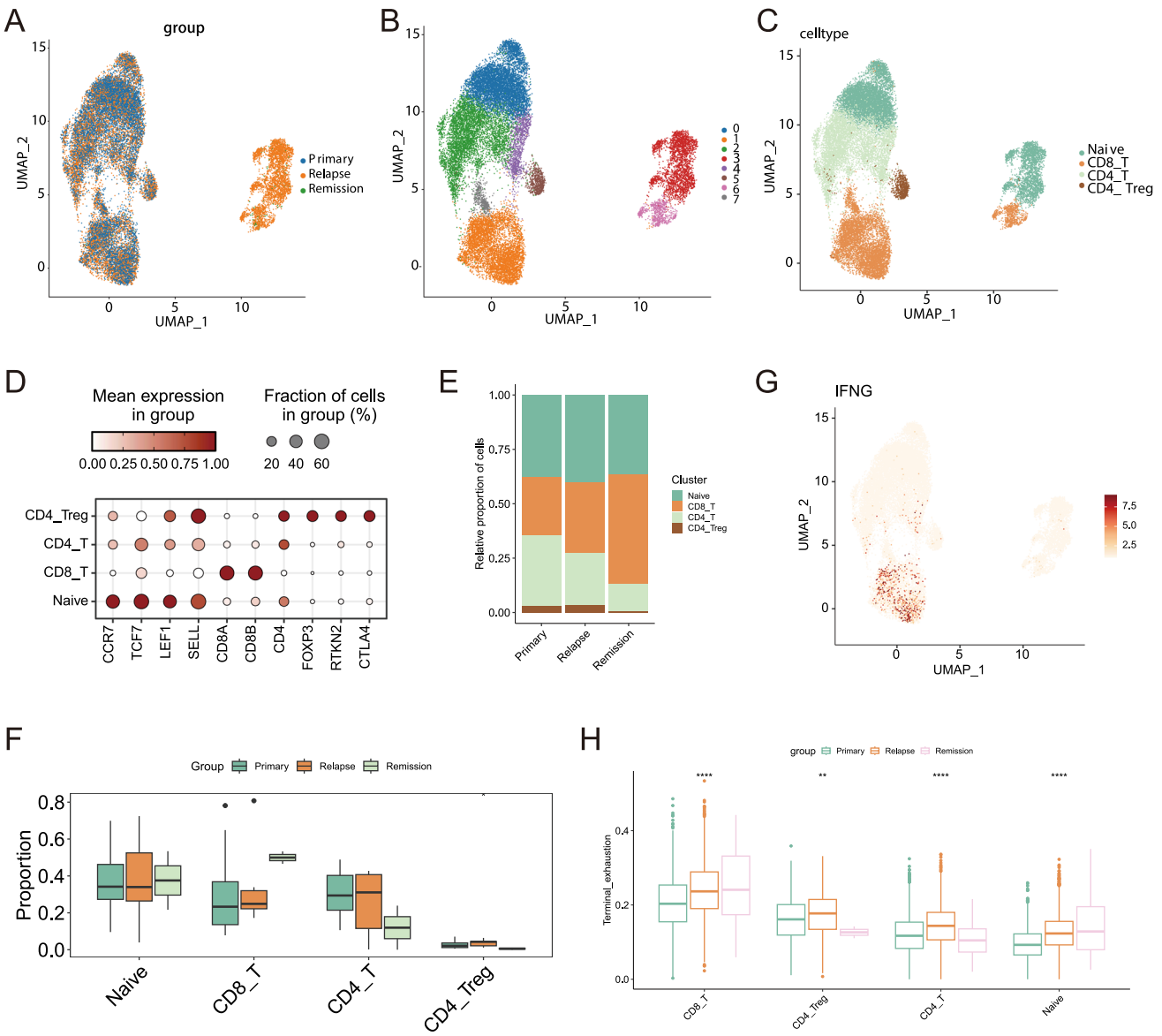

Fig. 2 Subclustering and annotation of T cells. **A** UMAP dimensionality reduction analysis showing the distribution of T cells in primary, remission, and relapsed MM samples. **B** UMAP dimensionality reduction analysis displaying the clustering results of T cells. **C** The results of the annotation of T cell subpopulations. **D** The expression of marker genes in different T cell subpopulations. **E** The proportion of T cell subpopulations in primary, remission, and relapsed MM samples. **F** The proportion differences of various cells in primary, remission, and relapsed MM samples. **G** The expression patterns of subtype-specific genes in T cell subsets from primary, remission, and relapsed MM samples. The size of each bubble represents the proportion of T cell subtypes expressing the gene. The color intensity of the bubbles represents the normalized value of gene expression levels. **H** Exhaustion scores of T cells across different T cell types in the different groups. * $p<0.05$

Immune cell transcriptional remodeling in MM relapse: coordinated NF-κB suppression and altered functional states

Building upon our initial findings regarding cellular composition and intergroup disparities (Fig. 1A), we observed that besides T cells, CD14+monocytes and plasma cells represented the most abundant immune populations within the TME, exhibiting significantly higher proportions in the primary group compared to the relapse cohort. Of particular relevance, seminal studies have established that plasma cells—the malignant origin of MM—arise from terminal differentiation of B cells [19]. Given these pivotal observations, the current investigation will primarily focus on elucidating the mechanistic contributions of CD14+monocytes, plasma cells, and their B cell precursors in MM relapse

pathogenesis. Through comprehensive differential gene expression profiling and functional enrichment analyses, we aim to delineate the molecular signatures and biological functions of these immune subsets during disease progression. In plasma cells, comparative analysis between primary and relapsed groups identified 837 DEGs, including 206 significantly upregulated and 631 downregulated genes (Fig. 3A, relapsed vs. primary). Notably, Macrophage Migration Inhibitory Factor (MIF) ranked among the top five most significantly upregulated genes. Functional enrichment analysis demonstrated a clear functional divergence between up- and down-regulated genes. Up-regulated genes were predominantly enriched in metabolic processes, including protein processing in the endoplasmic reticulum, amino acid biosynthesis, and oxidative phosphorylation (Fig. 3B). In contrast, down-regulated genes were significantly associated with inflammatory pathways, most notably the NF-kappa B signaling pathway (Fig. 3C).

We subsequently conducted a sub-clustering analysis of CD14+and CD16+monocytes. Following dimensionality reduction and clustering, CD14+monocytes were categorized into three distinct clusters (Fig. S1A–S1B). Based on classical marker genes, the CD14+monocytes were further classified into three subtypes: CD14_Mono_HLA, CD14_Mono_CXCL8, and CD14_Mono_VSIR (Fig. S1C–S1D). Similarly, after dimensionality reduction and clustering, CD16+monocytes were annotated into three types: CD16_Mono_FCGR3A, CD16_Mono_LGALS2, and CD16_Mono_SIGLEC5 (Fig. S2A–S2D). All three subtypes of CD14+monocytes were identified across primary, remission, and relapsed MM samples (Fig. S1E–S1F, Fig. S2E–S2F). All three subtypes of CD14+and CD16+monocytes were detected across primary, remission, and relapsed MM samples (Fig. S1E–S1F, Fig. S2E–S2F). Among CD14+monocytes, a total of 433 DEGs were identified in the relapsed group compared to the primary group, with 266 genes being upregulated and 167 downregulated (Fig. 3D). The upregulated genes exhibited significant enrichment in leukocyte transendothelial migration (Fig. 3E), while the downregulated genes were notably enriched in inflammatory pathways, including the interferon gamma response, interferon alpha response, TNFα signaling via NF-κB, and inflammatory response pathways (Fig. 3F).

After dimensionality reduction and clustering, B cells were annotated into four types: Bm_FCRL5, Bcell_IGLL1, Bcell_IGKV3, and Bcell_IGHM (Fig. S3A–S3D). All four subtypes of B cells were detected across primary, remission, and relapsed MM samples (Fig. S3E–S3F). In B cells, a total of 214 DEGs were identified, with 148 being upregulated and 66 downregulated, when comparing the primary and relapsed groups (Fig. 3G, relapsed vs. primary). Functional enrichment analysis revealed that the upregulated genes were significantly enriched in leukocyte transendothelial migration (Fig. 3H), while the downregulated genes were significantly enriched in TNFα-NF-κB signaling (Fig. 3I). These findings reveal a recurrent pattern of NF-κB pathway suppression across CD14+monocytes, plasma cells, and B cells in relapsed MM. As NF-κB serves as a master transcriptional regulator governing immune activation, inflammatory responses, and cellular proliferation, its systemic downregulation suggests profound immunosuppression in the relapse microenvironment [20]. Moreover, particularly in CD14+monocytes, the coordinated attenuation of multiple inflammatory pathways (interferon responses, TNFα signaling, etc.) implies functional impairment in immune surveillance capabilities.

Additionally, we analyzed the upregulated and downregulated genes in plasma cells (Fig. S4A-S4B), CD14+monocytes (Fig. S4E-S4F), and B cells (Fig. S4I-S4J) from remission samples in comparison to primary samples, and conducted functional enrichment analysis. In plasma cells, the upregulated genes in remission samples were significantly enriched in heme metabolism (Fig. S4C), whereas the downregulated genes were significantly enriched in estrogen response late (Fig. S4D). In CD14+monocytes and B cells, the upregulated genes in remission samples showed significant enrichment in chemical carcinogenesis—reactive oxygen species (Fig. S4G, S4K), while the downregulated genes were notably enriched in inflammatory pathways such as TNFα signaling via NF-κB (Fig. S4H, S4L).

Single-cell trajectory analysis reveals MIF-mediated BCR and interferon signaling in relapsed plasma cells

Further investigation into the dynamic evolution of plasma cells revealed three distinct cellular states: State1 cells were identified as the potential starting point, which subsequently bifurcated at Branch point 1 into State2 cells developing along the right trajectory and State3 cells progressing along the left trajectory (Fig. 4A, B). Pseudotime trajectory analysis (Fig. 4C) demonstrated that a greater proportion of relapsed plasma cells resided in State2. Using the Branch Expression Analysis Modeling (BEAM), we identified the top 50 branch-dependent genes that play pivotal roles in regulating the differentiation process from pre-branch to post-branch cell fates (Cell fate1 and Cell fate2). These genes were further classified into four expression modules (clusters) based on their expression patterns. Heatmap analysis (Fig. 4D) showed that Cluster2 exhibited progressively upregulated gene expression during the differentiation process from pre-branch to Cell fate1-State2 (right trajectory after Branch point 1), with MIF being notably enriched in this cluster. Pathway enrichment analysis revealed that

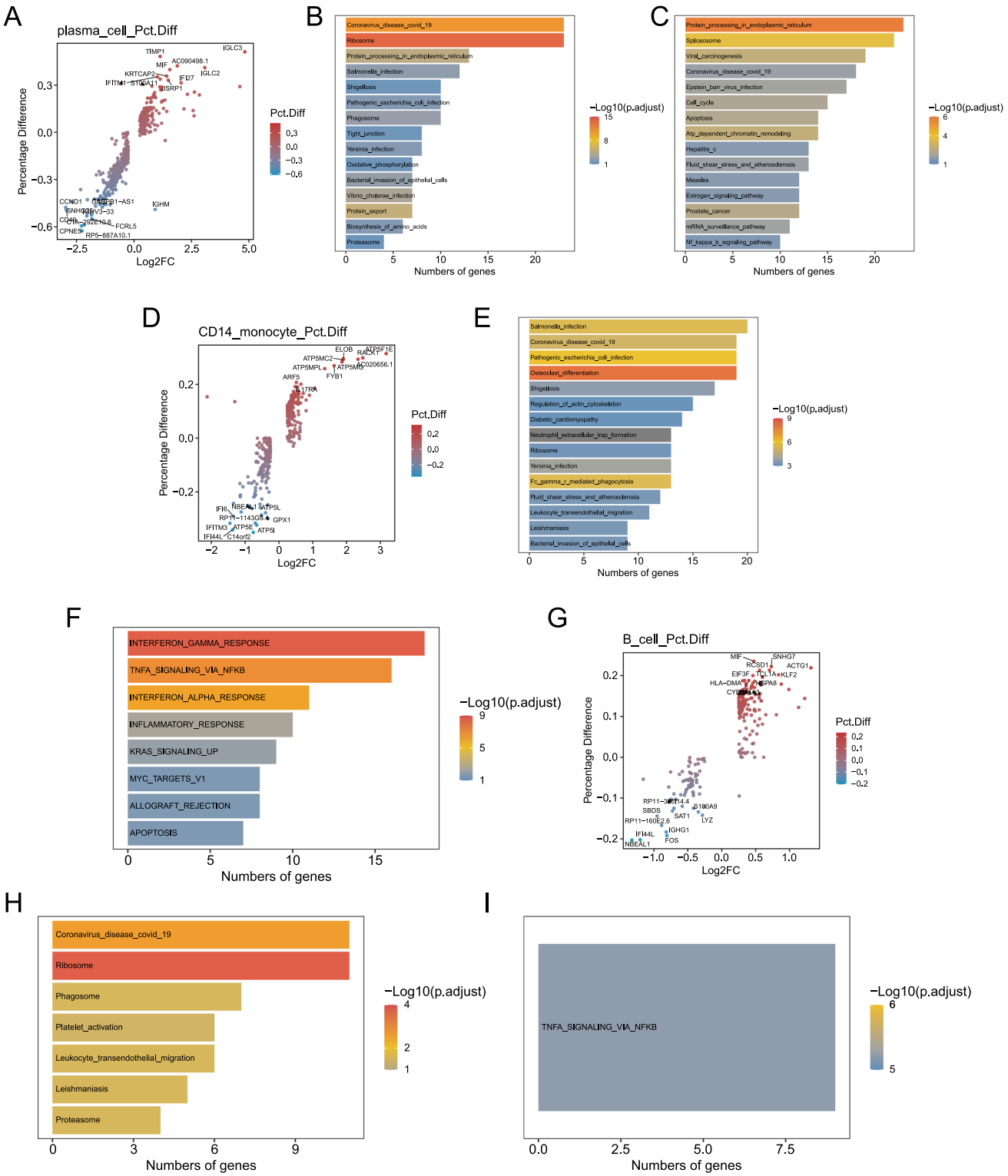

Cluster2 genes were primarily associated with the B cell receptor signaling pathway and interferon-alpha response signaling (Fig. 4E). These findings collectively demonstrate that MIF, along with the B cell receptor signaling pathway and interferon-alpha response, are significantly upregulated and play crucial roles during the differentiation of primary plasma cells into relapsed plasma cells.

Fig. 3 Differentially expressed genes and enrichment analysis in immune cells between primary and relapsed MM samples. **A** Differentially expressed genes between relapsed and primary MM groups in plasma cells. Genes upregulated in the relapsed MM samples are shown in red, while downregulated genes are shown in blue. **B** Enrichment analysis of upregulated genes in relapsed vs. primary plasma cells. **C** Enrichment analysis of downregulated genes in relapsed vs. primary plasma cells. **D** Differentially expressed genes between relapsed and primary MM groups in CD14 + monocytes. Genes upregulated in the relapsed MM samples are shown in red, while downregulated genes are shown in blue. **E** Enrichment analysis of upregulated genes in relapsed vs. primary CD14 + monocytes. **F** Enrichment analysis of downregulated genes in relapsed vs. primary CD14 + monocytes. **G** Differentially expressed genes between relapsed and primary MM groups in B cells. Genes upregulated in the relapsed MM samples are shown in red, while downregulated genes are shown in blue. **H** Enrichment analysis of upregulated genes in relapsed vs. primary B cells. **I** Enrichment analysis of downregulated genes in relapsed vs. primary B cells

Plasma cells exhibit distinct communication reprogramming between primary and relapsed MM microenvironments

To decipher intercellular communication within the TME, we constructed cell interaction networks quantifying potential receptor-ligand pairs in both primary (Fig. 5A), relapsed (Fig. 5B), and remission (Fig. 5C) MM groups. In the relapsed group, the interaction values of certain cell pairs reached approximately 20, while the highest value in the Primary group was only about 8 (Fig. 5A-B). This suggests that in the relapsed state, specific immune cells serving as signal senders exert a stronger influence on other cells. Compared to the primary group, the overall intercellular interaction intensity was elevated in the relapsed group, indicating significantly enhanced signal communication among certain immune cells (Fig. 5A-B). This phenomenon may be associated with the remodeling of the immune microenvironment and the enhancement or dysregulation of immune responses during tumor relapse. Heatmap analysis of differential intercellular signaling pathway strength (Fig. 5D-F) revealed that the MIF pathway exhibited stronger signal output from plasma cells in relapsed MM compared to primary MM. Furthermore, comparative analysis of signal input/output strength across cell subtypes (Fig. 5G-H) demonstrated that CD8 + T cells in the relapsed group showed enhanced signal reception capacity relative to the primary group.

We next focused our analysis on plasma cells as signal-sending cells and identified distinct group-specific communication patterns through systematic ligand-receptor pair analysis (Fig. 5J). In the relapsed group, plasma cells demonstrated enhanced interactions with most immune cell populations via amplified MIF pathway signaling. By contrast, primary group plasma cells preferentially engaged specific immune subsets through two distinct mechanisms: ICAM pathway-mediated interactions with CD8 + T cells, CD14 + monocytes, NK cells, neutrophils, and megakaryocytes, along with CD99-dependent communication involving CD8 + T cells, CD14 + monocytes, NK cells, CD16 + monocytes, mDCs, megakaryocytes, and pDCs. These findings collectively demonstrate a fundamental functional divergence in plasma cells between primary and relapsed TME, characterized by distinct ligand-receptor interaction patterns and pathway-specific communication strategies.

Oncogenic MIF signaling promotes immune evasion in relapsed MM via CD8 + T cell exhaustion and cytokine suppression

The above results showed that during the transition from in situ to relapsed plasma cells, the MIF gene, B cell receptor signaling pathway, and interferon-alpha response (IFN-α response) were significantly upregulated and played pivotal roles. In the relapsed group, plasma cells exhibited enhanced MIF signaling pathway activity, facilitating extensive crosstalk with multiple immune cell populations. Notably, CD8 + T cells displayed markedly increased signal reception intensity, reinforcing the central role of the MIF pathway in modulating the immunosuppressive TME.

Thus, we conducted a comparative analysis of tumor-associated immune features between primary and relapsed MM tissues, focusing on macrophage MIF expression and the functional state of tumor-infiltrating CD8 + T cells. Immunohistochemical analysis revealed that MIF expression was significantly elevated in relapsed MM samples compared to primary lesions (Fig. 6A, B). Flow cytometry was used to characterize the immune contexture in the tumor microenvironment. In relapsed MM, we observed that the level of CD8 + T cell infiltration was notably decreased compared to primary cases (Fig. 6C). More importantly, these CD8 + T cells displayed a functionally impaired phenotype, as evidenced by their markedly reduced production of the key effector cytokines IFN-γ and TNF-α (Fig. 6D-F). Taken together, these findings suggest that MM relapse is associated with a distinct immunological profile: upregulation of MIF co-occurs with a contracted and functionally exhausted CD8 + T cell compartment. This altered immune state likely contributes to an immunosuppressive tumor microenvironment that may promote disease progression and immune evasion.

Discussion

Our single-cell transcriptomic analysis reveals profound TME remodeling in relapsed MM, characterized by MIF-driven immune evasion, NF-κB pathway suppression, and

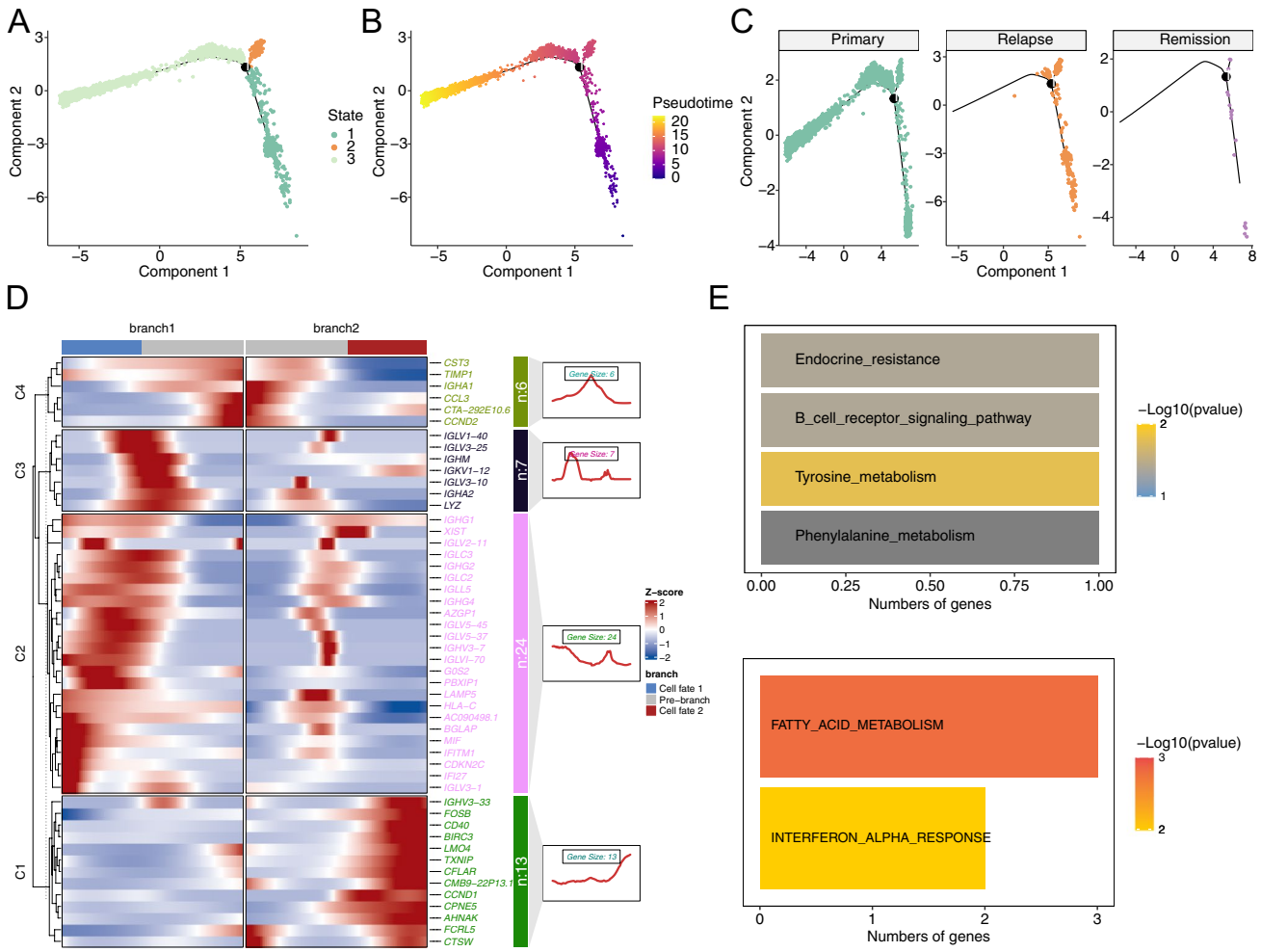

Fig. 4 Trajectory analysis of plasma cell subtypes. **A** Cell state trajectory colored by differentiation state. **B** Pseudotemporal ordering of cells (color-coded by pseudotime). **C** Trajectory colored by experimental groups. **D** Heatmap showing dynamic gene expression patterns along pseudotime. **E** Functional enrichment results for Cluster 2. (Top) KEGG pathway analysis; (Bottom) HALLMARK gene set enrichment

CD8+T cell dysfunction. These findings provide mechanistic insights into the immunosuppressive TME of relapsed MM and highlight potential therapeutic vulnerabilities.

Compared to primary MM, relapsed disease showed a pronounced shift in immune composition, with T cell enrichment and concomitant plasma cell depletion. This shift likely reflects dynamic immune remodeling and TME modulation. Further subclustering analysis suggested a compositional shift in the T cell landscape between remission and relapsed MM samples, with an observable trend toward higher enrichment of CD8+T cells in remission samples and a predominance of Tregs in relapsed samples. Prior studies indicate that CD8+T cells from remission MM patients exhibit restored functional and metabolic activity, a phenotype absent in relapsed cases [21], suggesting stage-specific roles for these subsets. Functional profiling demonstrated that CD8+T cells from primary MM patients expressed significantly higher levels of the cytotoxic marker IFNγ compared to relapsed patients [22], implying greater tumor-killing capacity. In contrast, relapsed MM CD8+T cells showed impaired function, marked by reduced IFNγ production [22]. This suppression may be driven by upregulated immune checkpoint molecules (e.g., PD-1, TIGIT) in the relapsed TME [23]. Concurrently, the expansion of Tregs in relapse [24] likely exacerbates immunosuppression via inhibitory cytokines (e.g., TGF-β, IL-10) or direct suppression of effector T cells [25], fostering immune escape. Collectively, these findings highlight stage-dependent alterations in T cell subsets. Remission MM is characterized by robust anti-tumor immunity mediated by CD8+T cells, while relapse is associated with Treg-driven suppression and CD8+T cell dysfunction. Therapeutic strategies targeting these T cell dynamics may improve outcomes in MM.

In patients with primary MM, the proportions of CD14+monocytes and plasma cells were significantly elevated compared to relapsed MM cases, suggesting these

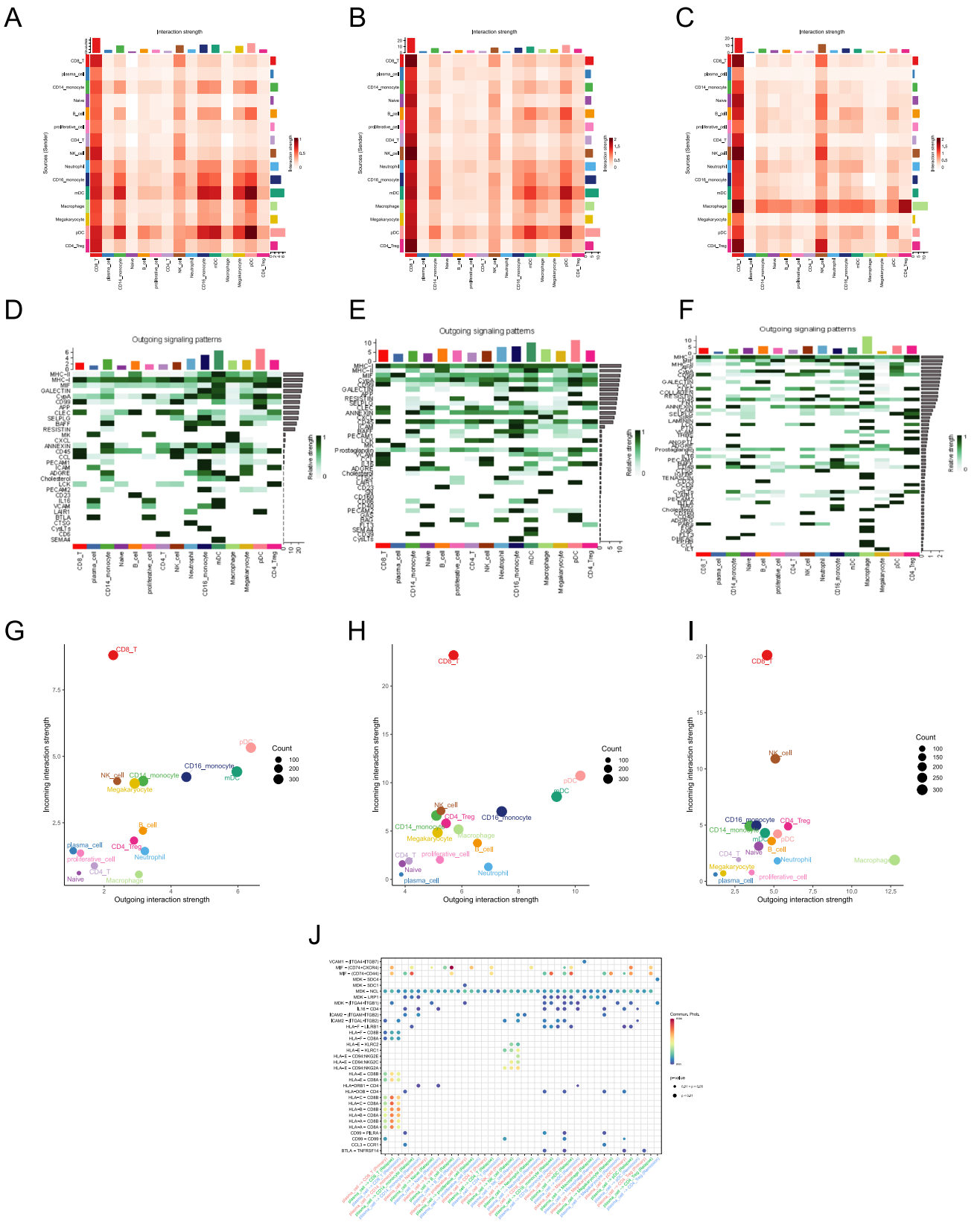

Fig. 5 Cell–cell interactions in the MM microenvironment. **A-C** Heatmaps depicting overall interaction strengths between specific cell subtypes in primary **(A)**, relapsed **(B)**, and remission **(C)** MM samples. **D-F** Heatmaps showing differential outgoing signaling pathway strengths between cell types in primary **(D)**, relapsed **(E)**, and remission **(F)** MM groups. **G-I** Dot plots displaying output and input signaling intensities across cell populations in primary **(G)**, relapsed **(H)**, and remission **(I)** MM samples. **J** Bubble plot highlighting differential ligand-receptor interactions between plasma cells (sender cells) and immune cells in primary vs. relapsed MM

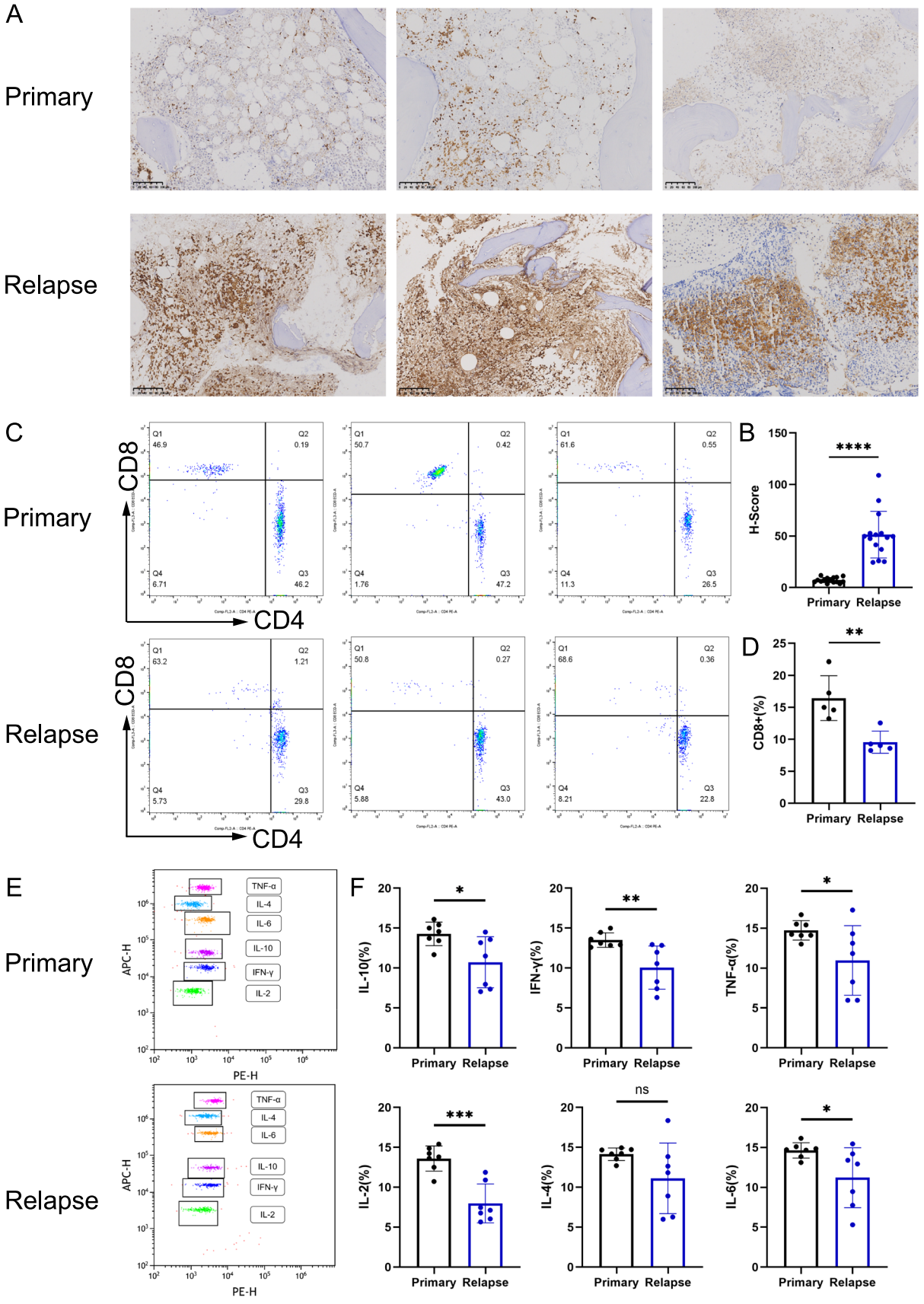
A
Primary
Relapse
C
Primary
Relapse
CD8
CD4
Q1 46.9
Q2 0.19
Q4 6.71
Q3 46.2
Q1 50.7
Q2 0.42
Q4 1.76
Q3 47.2
Q1 61.6
Q2 0.55
Q4 11.3
Q3 26.5
Q1 63.2
Q2 1.21
Q4 5.73
Q3 29.8
Q1 50.8
Q2 0.27
Q4 5.88
Q3 43.0
Q1 68.6
Q2 0.36
Q4 8.21
Q3 22.8
B
H-Score
****
Primary Relapse
D
CD8+(%)
**
Primary Relapse
E
Primary
Relapse
APC-H
PE-H
TNF-α
IL-4
IL-6
IL-10
IFN-γ
IL-2
F
IL-10(%)
*
IFN-γ(%)
**
TNF-α(%)
*
IL-2(%)
***
IL-4(%)
ns
IL-6(%)
*
Primary Relapse

Fig. 6 Elevated MIF expression and reduced CD8+T cell/IFN-γ/TNF-α levels in relapsed MM tissues. **A** Representative immunohistochemical (IHC) staining of MIF in primary(n=5) and relapsed(n=5) MM tissues (scale bar: 100 μm), Three fields of view were selected from each histopathological section. **B** Quantitative H-score analysis of MIF staining intensity in normal tissue and MM tissue.****$p<0.0001$. **C** Flow cytometry analysis of CD8+T cell infiltration frequencies in primary(n=5) and relapsed(n=5) MM tissues. **D** The statistical analysis of the proportion of CD8+T cells in primary and relapsed MM samples. Data presented as mean±SD; **$p<0.01$. **E** Flow cytometry quantification of IFN-γ and TNF-α levels in primary(n=7) and relapsed(n=7) MM tissues. **F** The statistical analysis of the levels of IFN-γ and TNF-α in primary and relapsed MM samples. Data presented as mean±SD; *$p<0.05$, **$p<0.01$, ***$p<0.001$

cell populations may exhibit enhanced biological activity during early disease stages. As key immune regulators, CD14+monocytes may drive enhanced inflammatory responses in the tumor microenvironment, potentially contributing to disease progression and osteolytic events [26]. Notably, our analyses revealed significant suppression of NF-κB signaling in plasma cells, CD14+monocytes, and B cells [27]. Given the central role of NF-κB in inflammatory responses and immune regulation, its inhibition may profoundly alter cellular function. In plasma cells and B cells, NF-κB suppression could impair proliferation, differentiation, and survival capacity, potentially explaining their reduced prevalence in relapsed MM [26–28]. Furthermore, NF-κB inhibition may attenuate the release of critical inflammatory mediators such as IL-6 and TNF-α, which are known to drive MM pathogenesis [29, 30]. Mechanistically, NF-κB pathway suppression has been shown to significantly inhibit MM cell proliferation, migration, and osteoclastogenic activity [31–33]. For instance, LGR4-mediated activation of NF-κB promotes tumor homing and bone destruction, while pharmacological inhibition of this pathway reverses these effects [31]. Similarly, VCP20 exerts anti-tumor effects through NF-κB suppression [32]. However, the observed reactivation of NF-κB signaling in relapsed MM may contribute to acquired drug resistance and immune evasion [34], highlighting the dynamic regulation of this pathway during disease evolution. Accordingly, the expansion of CD14+monocytes and plasma cells coupled with NF-κB suppression in primary MM may represent a coordinated mechanism of early disease regulation. Elucidating these pathways could unveil novel therapeutic targets for MM intervention.

Our investigation of plasma cell dynamics identified significant upregulation of MIF in relapsed MM samples. IHC analysis further confirmed elevated MIF expression in relapsed versus primary MM tissues. Pseudotime trajectory analysis established MIF as a key regulator of plasma cell evolution, mechanistically linked to both BCR and IFN-α signaling pathways. Notably, flow cytometry revealed significantly reduced IFN-γ and TNF-α levels in relapsed compared to primary MM tissues, suggesting an altered inflammatory microenvironment during disease progression. As a pleiotropic cytokine, MIF orchestrates immune regulation, inflammatory responses, and tumor progression, with its overexpression in MM correlating strongly with disease advancement and poor prognosis [35]. Mechanistically, MIF promotes tumor cell survival and drug resistance by modulating apoptosis, proliferation, and migratory capacity [36], with its elevated expression in relapsed cases suggesting critical roles in microenvironmental adaptation, immune evasion, and acquired treatment resistance [37, 38]. The BCR pathway—central to B-cell and plasma cell development—appears co-opted by MIF through regulation of key components like SYK and PI3K [39], potentially amplifying BCR signal transduction to bolster tumor cell survival[40]. Concurrently, MIF engages with IFN-α signaling by modulating STAT1 and IRF4 [41, 42], shaping both immunoregulatory responses and tumor microenvironment remodeling. This dual-pathway integration likely facilitates immune escape during relapse [43].

Our cell communication analysis revealed enhanced signaling reception in $CD8^+$ T cells from relapsed MM samples, where plasma cells exhibited intensified MIF-mediated interactions with immune cells (particularly CD8+T cells). Flow cytometry demonstrated increased CD8+T cell infiltration but decreased IFN-γ levels in relapsed versus primary MM tissues. The augmented signal reception capacity of these CD8+T cells likely reflects functional reprogramming affecting their antitumor responses [44]. Mechanistically, plasma cell-derived MIF signaling appears to modulate CD8+T cell function by suppressing cytotoxicity and promoting exhaustion [44], creating an immune-permissive microenvironment that facilitates tumor immune evasion and disease progression [45]. Although numerically expanded, these CD8+T cells exhibit functional impairment characteristic of tumor microenvironment-induced exhaustion [46, 47], with MIF signaling further compromising their cytotoxic potential [48]. Notably, MIF downregulates NKG2D expression and IFN-γ production in CD8+T cells [49], representing a key mechanism underlying immune dysfunction in MM relapse. Collectively, these findings establish a paradigm where MIF-mediated crosstalk between plasma cells and numerically expanded but functionally impaired CD8+T cells drives disease recurrence, highlighting this axis as a promising therapeutic target for relapsed MM.

This study delineates profound remodeling of the TME in relapsed MM through single-cell transcriptomic profiling, revealing MIF-mediated immune evasion, suppression of NF-κB signaling, and functional exhaustion of CD8+T cells. Our findings demonstrate an increased proportion of immunosuppressive Tregs alongside numerically expanded

but functionally impaired CD8+T cells in relapsed MM, characterized by diminished production of IFN-γ and TNF-α. Furthermore, systemic inhibition of the NF-κB pathway in plasma cells, CD14+monocytes, and B cells exacerbates the immunosuppressive TME. Mechanistically, MIF emerges as a pivotal regulator driving plasma cell evolution via activation of BCR and interferon-alpha signaling pathways while reinforcing crosstalk with CD8+T cells, thereby promoting disease relapse. These insights not only elucidate the immune escape mechanisms underlying MM recurrence but also provide a rationale for therapeutic strategies targeting the MIF pathway or restoring CD8+T cell function. Future investigations should explore the translational potential of MIF blockade in clinical interventions to overcome immune suppression and improve outcomes in relapsed MM.

Supplementary Information The online version contains supplementary material available at https://doi.org/10.1007/s10238-026-02113-7.

Acknowledgements Not applicable.

Author contributions Jing Ma: Data curation, Writing- Original draft preparation. Shuang Gao: Visualization, Investigation. Zhigang Zhao and Qian Li: Supervision, Funding acquisition. Su Liu: Software, Validation. Lin Chen: Writing- Reviewing and Editing. Li Lin: Conceptualization, Methodology, Software. Zhiying Zhang: Conceptualization, Methodology.

Funding This study was funded by the National Natural Science Foundation of China (grant 81870150), the National Natural Science Foundation of China (grant 81670102), and the National Natural Science Foundation of China (grant 82000216),Tianjin Key Medical Discipline Construction Project (grant TJYXZDXK-3-003A).

Data availability The datasets presented in this study can be found in online repositories. The names of the repository/repositories and accession number(s) can be found in the article/Supplementary Material. All data are available from the GEO (https://ncbi.nlm.nih.gov/geo/) database within the article. GEO database under accession number GSE223060.

Declarations

Competing interests The authors declare no competing interests.

Ethical approval The study was conducted according to the principles expressed in the Declaration of Helsinki and was approved by the Ethics Committee of This study has garnered approval from Medical Ethics Committee of Tianjin Cancer Hospital Airport Hospital (IREC number: LWK-2025–0012). Written informed consent was obtained from all patients.

Consent for publication Not applicable.

References

1. Vo JN, Wu YM, Mishler J, Hall S, Mannan R, Wang L, et al. The genetic heterogeneity and drug resistance mechanisms of relapsed refractory multiple myeloma. Nat Commun. 2022;13(1):3750.
2. de Van Donk N, Pawlyn C, Yong KL. Multiple myeloma. Lancet (London, England). 2021;397(10272):410–27.
3. Siegel RL, Giaquinto AN, Jemal A. Cancer statistics, 2024. CA Cancer J Clin. 2024;74(1):12–49.
4. Dimopoulos MA, Merlini G, Bridoux F, Leung N, Mikhael J, Harrison SJ, et al. Management of multiple myeloma-related renal impairment: recommendations from the International Myeloma Working Group. Lancet Oncol. 2023;24(7):e293–311.
5. Podar K, Leleu X. Relapsed/refractory multiple myeloma in 2020/2021 and beyond. Cancers (Basel). 2021. https://doi.org/10.3390/cancers13205154.
6. Li S, Liu J, Peyton M, Lazaro O, McCabe SD, Huang X, et al. Multiple myeloma insights from single-cell analysis: clonal evolution, the microenvironment, therapy evasion, and clinical implications. Cancers (Basel). 2025. https://doi.org/10.3390/cancers17040653.
7. De Novellis D, Scala P, Giudice V, Selleri C. High-risk genetic multiple myeloma: from molecular classification to innovative treatment with monoclonal antibodies and T-cell redirecting therapies. Cells. 2025. https://doi.org/10.3390/cells14110776.
8. Wu H, Guo C, Wang C, Xu J, Zheng S, Duan J, et al. Single-cell RNA sequencing reveals tumor heterogeneity, microenvironment, and drug-resistance mechanisms of recurrent glioblastoma. Cancer Sci. 2023;114(6):2609–21.
9. Chen Z, Zhang T, Li W, Hu J, Ou Y, Ye F, et al. Single-cell RNA sequencing analysis reveals the dynamic changes in the tumor microenvironment during NMIBC recurrence. Apoptosis Intern J Program Cell Death. 2025;30(1–2):282–96.
10. Li X, Lin Z, Zhao F, Huang T, Fan W, Cen L, et al. Unveiling the cellular landscape: insights from single-cell RNA sequencing in multiple myeloma. Front Immunol. 2024;15:1458638.
11. Cheng Y, Sun F, Alapat DV, Wanchai V, Mery D, Siegel ER, et al. Multi-omics reveal immune microenvironment alterations in multiple myeloma and its precursor stages. Blood Cancer J. 2024;14(1):194.
12. Wang Y, Peng Y, Yang C, Xiong D, Wang Z, Peng H, et al. Single-cell sequencing analysis of multiple myeloma heterogeneity and identification of new theranostic targets. Cell Death Dis. 2024;15(9):672.
13. Cohen YC, Zada M, Wang SY, Bornstein C, David E, Moshe A, et al. Identification of resistance pathways and therapeutic targets in relapsed multiple myeloma patients through single-cell sequencing. Nat Med. 2021;27(3):491–503.
14. Long X, Li F, Tang S, Liu J, Fu Y, Feng Y. ScRNA-Seq and bulk-seq analysis identifies S100A9 plasma cells as a potentially

effective immunotherapeutic agent for multiple myeloma. J Inflamm Res. 2024;17:1527–48.
15. Tirier SM, Mallm JP, Steiger S, Poos AM, Awwad MHS, Giesen N, et al. Subclone-specific microenvironmental impact and drug response in refractory multiple myeloma revealed by single-cell transcriptomics. Nat Commun. 2021;12(1):6960.
16. Korsunsky I, Millard N, Fan J, Slowikowski K, Zhang F, Wei K, et al. Fast, sensitive and accurate integration of single-cell data with Harmony. Nat Methods. 2019;16(12):1289–96.
17. Yu G, Wang LG, Han Y, He QY. ClusterProfiler: an R package for comparing biological themes among gene clusters. OMICS. 2012;16(5):284–7.
18. Qiu X, Mao Q, Tang Y, Wang L, Chawla R, Pliner HA, et al. Reversed graph embedding resolves complex single-cell trajectories. Nat Methods. 2017;14(10):979–82.
19. Barwick BG, Gupta VA, Vertino PM, Boise LH. Cell of origin and genetic alterations in the pathogenesis of multiple myeloma. Front Immunol. 2019;10:1121.
20. Mao H, Zhao X, Sun SC. NF-κB in inflammation and cancer. Cell Mol Immunol. 2025. https://doi.org/10.1038/s41423-025-01310-w.
21. Gudgeon N, Giles H, Bishop EL, Fulton-Ward T, Escribano-Gonzalez C, Munford H, et al. Uptake of long-chain fatty acids from the bone marrow suppresses CD8+ T-cell metabolism and function in multiple myeloma. Blood Adv. 2023;7(20):6035–47.
22. Hoekstra ME, Slagter M, Urbanus J, Toebes M, Slingerland N, de Rink I, et al. Distinct spatiotemporal dynamics of CD8(+) T cell-derived cytokines in the tumor microenvironment. Cancer Cell. 2024;42(1):157-67.e9.
23. Zhao K, Ren C, Tang D, Zhao L, Chen X, Wang Y, et al. The altering cellular components and function in tumor microenvironment during remissive and relapsed stages of anti-CD19 CAR T-cell treated lymphoma mice. Front Immunol. 2023;14:1101769.
24. Kawano Y, Zavidij O, Park J, Moschetta M, Kokubun K, Mouhieddine TH, et al. Blocking IFNAR1 inhibits multiple myeloma-driven Treg expansion and immunosuppression. J Clin Investig. 2018;128(6):2487–99.
25. Hadjiaggelidou C, Katodritou E. Regulatory T-cells and multiple myeloma: implications in tumor immune biology and treatment. J Clin Med. 2021. https://doi.org/10.3390/jcm10194588.
26. Sun J, Park C, Guenthner N, Gurley S, Zhang L, Lubben B, et al. Tumor-associated macrophages in multiple myeloma: advances in biology and therapy. J Immunother Cancer. 2022. https://doi.org/10.1136/jitc-2021-003975.
27. Yi H, Liang L, Wang H, Luo S, Hu L, Wang Y, et al. Albendazole inhibits NF-κB signaling pathway to overcome tumor stemness and bortezomib resistance in multiple myeloma. Cancer Lett. 2021;520:307–20.
28. Peng F, Liu Z, Jiang F, Li N, Wang H, Meng N, et al. T-lymphocytes suppression by CD14(+) monocytes with high expression of ULK2 in patients with multiple myeloma. J Transl Med. 2025;23(1):511.
29. Li J, Liu Y, Cao Y, Wang J, Zhao X, Jiao J, et al. Inhibition of miR-155 attenuates CD14(+) monocyte-mediated inflammatory response and oxidative stress in psoriasis through TLR4/MyD88/NF-κB signaling pathway. Clin Cosmet Investig Dermatol. 2022;15:193–201.
30. Wong AH, Shin EM, Tergaonkar V, Chng WJ. Targeting NF-κB signaling for multiple myeloma. Cancers (Basel). 2020. https://doi.org/10.3390/cancers12082203.
31. He N, Yang Q, Li Z, Guo J, Kuang C, Zhu Y, et al. LGR4 promotes proliferation and homing via activation of the NF-κB signaling pathway in multiple myeloma. Int J Oncol. 2025. https://doi.org/10.3892/ijo.2025.5718.
32. Wei R, Cao Y, Wu H, Liu X, Jiang M, Luo X, et al. Inhibition of VCP modulates NF-κB signaling pathway to suppress multiple myeloma cell proliferation and osteoclast differentiation. Aging Albany NY. 2023;15(16):8220–36.
33. Yao Y, Zhang Y, Shi M, Sun Y, Chen C, Niu M, et al. Blockade of deubiquitinase USP7 overcomes bortezomib resistance by suppressing NF-κB signaling pathway in multiple myeloma. J Leukoc Biol. 2018;104(6):1105–15.
34. Yang L, Chen J, Han X, Zhang E, Huang X, Guo X, et al. Pirh2 mediates the sensitivity of myeloma cells to bortezomib via canonical NF-κB signaling pathway. Protein Cell. 2018;9(9):770–84.
35. Li D, Qiao B, Cheng Q, Chen L, Zhao F, Zuo L, et al. Macrophage migration inhibitory factor as a prognostic biomarker in multiple myeloma: clinical significance and in vitro effects. Carcinog. 2025. https://doi.org/10.1093/carcin/bgaf033.
36. Sharaf-Eldein M, Elghannam D, Elderiny W, Abdel-Malak C. Prognostic implication of MIF gene expression in childhood acute lymphoblastic leukemia. Clin Lab. 2018;64(9):1429–37.
37. Visram A, Dasari S, Anderson E, Kumar S, Kourelis TV. Relapsed multiple myeloma demonstrates distinct patterns of immune microenvironment and malignant cell-mediated immunosuppression. Blood Cancer J. 2021;11(3):45.
38. Piddock RE, Marlein CR, Abdul-Aziz A, Shafat MS, Auger MJ, Bowles KM, et al. Myeloma-derived macrophage inhibitory factor regulates bone marrow stromal cell-derived IL-6 via c-MYC. J Hematol Oncol. 2018;11(1):66.
39. Park GB, Kim YS, Lee HK, Yang JW, Kim D, Hur DY. ASK1/JNK-mediated TAp63 activation controls the cell survival signal of baicalein-treated EBV-transformed B cells. Mol Cell Biochem. 2016;412(1–2):247–58.
40. Alampour-Rajabi S, El Bounkari O, Rot A, Müller-Newen G, Bachelerie F, Gawaz M, et al. MIF interacts with CXCR7 to promote receptor internalization, ERK1/2 and ZAP-70 signaling, and lymphocyte chemotaxis. FASEB J. 2015;29(11):4497–511.
41. Cook SL, Franke MC, Sievert EP, Sciammas R. A synchronous IRF4-dependent gene regulatory network in B and helper T cells orchestrating the antibody response. Trends Immunol. 2020;41(7):614–28.
42. Holzgruber J, Martins C, Kulcsar Z, Duplaine A, Rasbach E, Migayron L, et al. Type I interferon signaling induces melanoma cell-intrinsic PD-1 and its inhibition antagonizes immune checkpoint blockade. Nat Commun. 2024;15(1):7165.
43. Swamydas M, Murphy EV, Ignatz-Hoover JJ, Malek E, Driscoll JJ. Deciphering mechanisms of immune escape to inform immunotherapeutic strategies in multiple myeloma. J Hematol Oncol. 2022;15(1):17.
44. Starbeck-Miller GR, Xue HH, Harty JT. IL-12 and type I interferon prolong the division of activated CD8 T cells by maintaining high-affinity IL-2 signaling in vivo. J Exp Med. 2014;211(1):105–20.
45. Pracha SH, Shrestha S, Ryan N, Upadhaya P, Lamenza FF, Jagadeesha S, et al. Targeting macrophage migration inhibitory factor to inhibit T cell immunosuppression in the tumor microenvironment and improve cancer outcomes in head and neck squamous cell carcinoma. Oral Oncol. 2025;160:107126.
46. Westhrin M, Blazevski J, Textor A, Abdollahi P, Gopalakrishnan RP, Ngo LT, et al. Id-neoantigen vaccine induces therapeutic CD8(+) T cells against multiple myeloma: H chain-loss escapees cause FLC MM. J Immunother Cancer. 2023. https://doi.org/10.1136/jitc-2023-006944.
47. Baessler A, Vignali DAA. T cell exhaustion. Annu Rev Immunol. 2024;42(1):179–206.
48. Zhou Q, Yan X, Gershan J, Orentas RJ, Johnson BD. Expression of macrophage migration inhibitory factor by neuroblastoma leads to the inhibition of antitumor T cell reactivity in vivo. J Invest Med. 2008;181(3):1877–86.

49. Zhang Z, Zhou X, Guo J, Zhang F, Qian Y, Wang G, et al. TA-MSCs, TA-MSCs-EVs, MIF: their crosstalk in immunosuppressive tumor microenvironment. J Transl Med. 2022;20(1):320.